First-principles theory of short-range order, electronic excitations, and spin polarization in Ni-V and Pd-V alloys

C. Wolverton and Alex Zunger

National Renewable Energy Laboratory, Golden, Colorado 80401

The short-range order (SRO) and long-range order (LRO) of Ni-V and Pd-V alloys are studied theoretically by a combination of first-principles calculations of Ising-like interaction energies (J_f) with a Monte Carlo solution of the Ising Hamiltonian. We find the following: (i) There are several compositions in these alloys for which the dominant wave vectors of LRO and those of SRO do not coincide, indicating that the low-temperature (T) LRO may not always be inferred from the high-T SRO. (ii) In Ni_3V and Pd_3V, the density of states at the Fermi level, $n(\epsilon_F)$, is much larger in $L1_2$ than in the stable $D0_{22}$ structure. This has two consequences: (a) thermal electron-hole excitations across ϵ_F are energetically more favorable in the $L1_2$ structure and lead to a T dependence of J_f, and (b) magnetic stabilization is larger in $L1_2$, so spin polarization affects structural stability. As a result, (iii) calculations using T-dependent J_f's are needed to obtain quantitative agreement with experimental measurements of LRO, SRO, and transition temperatures in $Ni_{0.75}V_{0.25}$, $Ni_{0.67}V_{0.33}$, and $Pd_{0.75}V_{0.25}$. (iv) We provide predictions of the SRO patterns where there is currently no experimental evidence for $Pd_{0.67}V_{0.33}$, $Ni_{0.6}V_{0.4}$, $Pd_{0.6}V_{0.4}$, and $Pd_{0.5}V_{0.5}$. (v) For Ni_3V and Pd_3V, discrepancies are found between the total-energy differences of the $L1_2$ and $D0_{22}$ structures as determined by $T=0$ first-principles calculations and those inferred from diffuse neutron scattering measurements at high T. By performing temperature-dependent self-consistent local-density-approximation calculations, we find that electronic excitations are responsible for reducing the discrepancy by $\sim 25\%$ and the combination of spin polarization and electronic excitations reduce the discrepancy by ~ 30–50%. Thus, electronic excitations and spin polarization are not fully responsible for the T dependence of J_f used in the SRO calculations.

I. INTRODUCTION

In many solid-state intermetallic alloys, an order-disorder transition marks a structural transformation from a low-temperature long-range ordered (LRO) state to a high-temperature short-range ordered (SRO) solid solution. Bragg diffraction and diffuse scattering in between Bragg peaks are often used to measure the degree and type of LRO and SRO, respectively, present in alloys. For a binary $A_{1-x}B_x$ alloy, any configuration of A and B atoms may be described by Ising-like spin variables, $\hat{S}_i = -1(+1)$ if site i is occupied by an $A(B)$ atom. The SRO is characterized in real space by the pair correlation function $\overline{\Pi}_{0,n}$ for the nth atomic shell, given by $\hat{S}_i\hat{S}_{i+n}$ averaged over all symmetry-equivalent pairs of lattice sites. The Warren-Cowley SRO parameter for shell n is then

$$\alpha_{SRO}(x,n) = \frac{\langle \overline{\Pi}_{0,n} \rangle - q^2}{1 - q^2} , \qquad (1)$$

where the brackets denote a thermal average, and $q = 2x - 1$. For a *completely random alloy*, the spins are uncorrelated, so $\langle \hat{S}_i\hat{S}_{i+n} \rangle = \langle \hat{S}_i \rangle \langle \hat{S}_{i+n} \rangle = q^2$, and hence $\alpha_{SRO}(x,n) = 0$ for all shells. Thus, the SRO parameters, $\alpha_{SRO}(x,n)$ measure the extent to which spatial *correlations* exist in disordered alloys. In diffraction experiments, these correlations give rise to intensity modulations in the monotonic Laue background between the Bragg peaks. Thus, the correlations in disordered alloys may be experimentally measured by extracting the portion of diffuse scattered intensity due to SRO, which is proportional to the lattice Fourier transform of $\alpha_{SRO}(x,n)$,

$$\alpha_{SRO}(x,\mathbf{k}) = \sum_{n}^{n_R} \alpha_{SRO}(x,n)e^{i\mathbf{k}\cdot\mathbf{R}_n} , \qquad (2)$$

where n_R is the number of real-space shells used in the transform.

A theoretical treatment that is commonly used to evaluate SRO is the mean-field Krivoglaz-Clapp-Moss formula,[1] which relates $\alpha_{SRO}(x,\mathbf{k})$ to $J_2(\mathbf{k})$, the lattice Fourier transform of the Ising-like effective *pair* interaction energies, $J_2(n)$ (between a site at the origin and one at the nth atomic shell):

$$\alpha_{SRO}(x,\mathbf{k}) = \frac{1}{1 + 4x(1-x)J_2(\mathbf{k})/kT}. \qquad (3)$$

The mean-field formula[2] of Eq. (3) guarantees that the wave vector at which the SRO peaks, $\mathbf{k}_{SRO}$, is given by the minimum of $J_2(\mathbf{k})$. Provided that there are no multibody (three or more sites) Ising-like interactions, the pair interaction $J_2(\mathbf{k})$ can also be used[3] to determine the energetically favorable low-temperature LRO states. Of-

tentimes (but not always[4]) the minimum of $J_2(\mathbf{k})$ also corresponds to the peak wave vector of the LRO state, $\mathbf{k}_{LRO}$ (e.g., as observed in Bragg diffraction). Thus, in many cases, the mean-field expectation[4] based on Eq. (3) is that the peak wave vectors of SRO and LRO coincide: $\mathbf{k}_{SRO} = \mathbf{k}_{LRO}$. This equivalence between $\mathbf{k}_{SRO}$ and $\mathbf{k}_{LRO}$ actually occurs in an overwhelming number of alloys.[5-7] In particular, a peak at $\mathbf{k}_{SRO} = \langle 000 \rangle$ indicates association of like atoms ("clustering") and is accompanied via Eq. (3) with phase-separating LRO, while an "off-Γ" ($\mathbf{k}_{SRO} \neq \langle 000 \rangle$) peak in α_{SRO} indicates association of unlike atoms ("anticlustering") and is accompanied by compound-forming LRO. Cases (i) ($\mathbf{k}_{SRO} = \mathbf{k}_{LRO} = \langle 000 \rangle$) and (iii) ($\mathbf{k}_{SRO} = \mathbf{k}_{LRO} \neq \langle 000 \rangle$) in Table I refer to these classic cases of clustering/phase-separating and anticlustering/compound-forming alloys, respectively. Sometimes it is assumed that this is *always* the case. For example, recent calculations of SRO in Ni-Pt by Pinski *et al.*[9] have been interpreted to imply LRO with the same underlying wave vectors.[10] Direct calculations of the LRO with the same nonrelativistic Hamiltonian showed,[11,12] however, that $\mathbf{k}_{SRO} \neq \mathbf{k}_{LRO}$.

Calculations that go beyond the mean-field approximation (such as those in this paper) use $J_2(\mathbf{k})$ in a *Monte Carlo* algorithm. The resulting $\mathbf{k}_{SRO}$ need not be related to $\mathbf{k}_{LRO}$. A number of possible relations between SRO and LRO wave vectors are enumerated in Table I. Cases involving "non-special-points," (ii)$_b$ and (iii)$_b$, are exemplified by Ni-Au (Refs. 13 and 14) and Cu-Pd (Refs. 15–17) alloys, respectively. In the Ni-Au system, the assessed composition-temperature phase diagram shows[18] a miscibility gap and total-energy calculations of many compounds give positive formation enthalpies,[14] both of which are clear indications of phase-separating tendencies ($\mathbf{k}_{LRO} = \langle 000 \rangle$); however, both recent first-principles calculations[14] and measured x-ray diffuse scattering[13] show ordering-type SRO ($\mathbf{k}_{SRO} \neq \langle 000 \rangle$), which peaks along the $\langle \zeta 00 \rangle$ line, with $\zeta = 0.6-$

0.8 (not at one of the special points listed in Table I). Thus, for Ni-Au, $\mathbf{k}_{SRO} \neq \mathbf{k}_{LRO}$. For Cu-Pd alloys, there are several compositions near Cu_3Pd for which the stable LRO structure is a long-period superstructure, which has dominant wave vectors along the $\langle 1\zeta 0 \rangle$ line, *between* the special points, $\langle 100 \rangle$ and $\langle 1\frac{1}{2}0 \rangle$. Experimental measurements[15] and first-principles calculations[16,17] both show $\mathbf{k}_{SRO}$, which is also split off of the special-point $\langle 100 \rangle$ along the $\langle 1\zeta 0 \rangle$ line.

In this paper, we examine theoretically the fcc-based LRO and SRO of the anticlustering/compound-forming alloys, Ni-V and Pd-V. Using a non-mean-field method (Monte Carlo simulated annealing) for determining the alloy SRO and LRO, we illustrate the cases (iii)$_a$, (iv)$_a$, (iv)$_b$, and (iv)$_c$ of Table I, which occur in these alloys. We show examples for which (iii)$_a$ the LRO and SRO wave vectors coincide [$Ni_{0.75}V_{0.25}$], (iv)$_{a,b,c}$ the LRO and SRO wave vectors are distinct [$Ni_{0.67}V_{0.33}$, $Ni_{0.50}V_{0.50}$, $Pd_{0.75}V_{0.25}$, $Pd_{0.67}V_{0.33}$, and $Pd_{0.50}V_{0.50}$], and (iv)$_{b,c}$ the wave vectors of either LRO or SRO occur at a non-special-point in the Brillouin zone [$Ni_{0.67}V_{0.33}$, $Ni_{0.50}V_{0.50}$, $Pd_{0.67}V_{0.33}$, and $Pd_{0.50}V_{0.50}$]. These examples demonstrate that there are clearly many exceptions to the mean-field expectation[4] of the correspondence between SRO and LRO wave vectors.

II. METHODOLOGY

We illustrate the methodology of our approach schematically in Fig. 1 ("approach I") and contrast it with the "inverse" problem ("approach II"). Here we only give the salient ideas of each method, and we refer the reader to Refs. 19 and 17, for more details of approach I, and to Ref. 20 for more details of approach II. In the method used in this paper (approach I), we begin by mapping a set of first-principles total energies $\{E_{tot}\}$ for a variety of ordered compounds onto an Ising-like cluster

TABLE I. Possible situations involving dominant wave vectors of long- and short-range order. "Off $\langle 000 \rangle$" refers to dominant wave vectors, which are not located at the origin, but occur at the special points of the Brillouin zone. The special points are defined as the points for which *any* $\mathbf{k}$-space function with the symmetry of the reciprocal lattice must have extrema, simply due to symmetry reasons. For example, for the direct-space fcc lattice (reciprocal-space bcc), the special points are (Ref. 8) $\langle 000 \rangle$, $\langle 100 \rangle$, $\langle 1\frac{1}{2}0 \rangle$, and $\frac{1}{2}\langle 111 \rangle$. $\mathbf{k}_{LRO} = \langle 000 \rangle$ indicates a phase-separating system, while $\mathbf{k}_{LRO} \neq \langle 000 \rangle$ refers to a compound-forming alloy. $\mathbf{k}_{SRO} = \langle 000 \rangle$ indicates a "clustering" solid solution (local association of like atoms), while $\mathbf{k}_{SRO} \neq \langle 000 \rangle$ refers to a solid solution which is "anticlustering" (local association of unlike atoms).

Case/type	$\mathbf{k}_{LRO}$	$\mathbf{k}_{SRO}$	Examples
(i)	$\langle 000 \rangle$	$\langle 000 \rangle$	Cu-Ni, Pd-Rh, $Ga_{1-x}Al_xAs$
(ii)$_a$	$\langle 000 \rangle$	off $\langle 000 \rangle$	Size-mismatched- III-V semiconductor alloys
(ii)$_b$	$\langle 000 \rangle$	non-special-point	Ni-Au
(iii)$_a$	off $\langle 000 \rangle$	off $\langle 000 \rangle$	Cu-Au, Ni_3V
(iii)$_b$	non-special-point	non-special-point	Cu_3Pd
(iv)$_a$	off $\langle 000 \rangle$	different off $\langle 000 \rangle$	Pd_3V
(iv)$_b$	off $\langle 000 \rangle$	non-special-point	$Pd_{0.5}V_{0.5}$
(iv)$_c$	non-special-point	off $\langle 000 \rangle$	Ni_2V, Pd_2V
(iv)$_d$	non-special-point	different non-special-point	?

	Input	Output
Approach I (First-principles input)	$\{E_{tot}^{(\sigma)}\} \xrightarrow{CE} \{J_f\}$	$\overset{MC}{\nearrow}$ Ground States $\overset{MC}{\longrightarrow} T_c$ $\overset{MC}{\searrow}$ SRO
Approach II (Measured SRO input)	SRO $\xrightarrow{MC^{-1}} \{J_f\}$	$\overset{MC}{\nearrow}$ Ground States $\overset{MC}{\longrightarrow} T_c$ $\overset{CE}{\searrow} \{E_{tot}^{(\sigma)}\}$
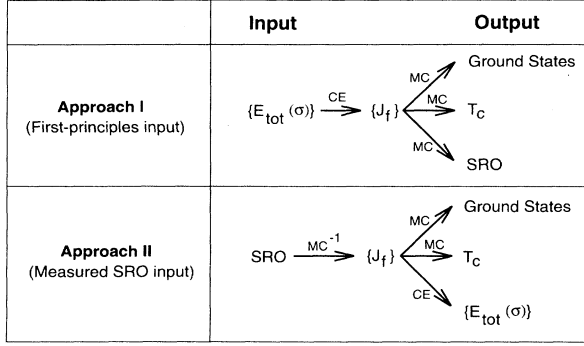
FIG. 1. Methodology used in this paper to deduce SRO, LRO, and transition temperatures from first-principles total energies (approach I). Also shown is the inverse approach (approach II) often used by experimental groups in which LRO, transition temperatures, and total energies are deduced from the measured diffuse intensity due to SRO. In both approaches, an intermediate step involves an Ising-like cluster expansion (CE) expressed in terms of effective interactions, J_f. "MC" refers to Monte Carlo calculations.

expansion involving effective interactions J_f for figures of lattice sites f (e.g., pairs, triplets, etc.). We emphasize that we are not limited to the case of effective *pair* interactions only. Once the set $\{J_f\}$ is obtained, it can be used in a Monte Carlo simulated annealing prescription, which provides a means to calculate (i) the $T=0$ LRO ground-state structures, (ii) the order-disorder transition temperatures T_c, as well as (iii) the alloy SRO.

Figure 1 also schematically depicts the inverse approach (approach II), which is often used by experimental researchers[20,5,21,6,22] who measure diffuse scattered intensity due to SRO. From the measured SRO pattern $\alpha_{SRO}(x, \mathbf{k})$, one may deduce a set of interaction parameters $\{J_f\}$ via an *inverse* procedure: Monte Carlo,[5,21–24] Krivoglaz-Clapp-Moss,[6] or cluster variation method.[20,25–27] These J_f's may then be used in a standard (not inverse) Monte Carlo to deduce the LRO, transition temperatures, or total-energy differences. The inverse approach is not generally valid for "case (ii)" alloys: Using SRO data showing anticlustering ("antiferromagnetic" J_f's) behavior, one cannot predict a phase-separating ("ferromagnetic") LRO. References 14 and 17 give the answer to this apparent paradox for transition metal[14] (Ni-Au) and semiconductor[17] (GaP-InP) case (ii) alloys.

In this paper, we use approach I with the following details: For Ni-V, the total energies of 24 fully relaxed structures as calculated from the linearized augmented plane wave (LAPW) method are mapped[28,14] onto 12 effective interactions J_f, while for Pd-V 18 total energies of unrelaxed structures from the method of linear muffin-tin orbitals are used to fit[28,29] 14 interactions. The set of $\{E_{tot}\}$ computed at $T=0$ is mapped onto an Ising-like Hamiltonian,[19] thereby extracting a set of $\{J_f\}$ at $T=0$. In these calculations, the total energy is a functional of the charge density $\rho(\mathbf{r})$ that is determined by summing all $|\Psi_i|^2$ (Ψ_i is the one-electron Kohn-Sham wave function

for state i) up to the Fermi energy, ϵ_F. This procedure may be generalized to finite T by allowing some occupied (unoccupied) states to exist above (below) ϵ_F. In other words, ϵ_F [or, more properly, the finite-T Fermi level, $\mu(T)$] can be computed from a *finite-T* Fermi distribution. The ensuing T dependence of $\rho(\mathbf{r}, T)$ propagates into E_{tot}, and thus into $\{J_f(T)\}$. We refer to this T dependence as the effect of electronic excitations on $\{J_f\}$, as was recently discussed[28] in the context of Ni$_3$V and Pd$_3$V. We report here computations involving the temperature-independent $\{J_f(T = 0)\}$, as well as computations that include a quadratic T dependence in several of the J_f's.[28] The contribution of electronic excitations and spin polarization to this T dependence is examined in Sec. IV.

In the Monte Carlo calculations presented here, we use a system size of $16^3 = 4096$ atoms with periodic boundary conditions for all SRO calculations. (For LRO computations, the system size is adjusted so as to be commensurate with the composition considered.) The SRO is determined using 500 Monte Carlo steps to equilibrate the system, and subsequently, averages are taken over at least 500 Monte Carlo steps. Thirty-five atomic shells [$n_R = 35$ in Eq. (2)] of $\alpha_{SRO}(x, n)$ are used in all SRO calculations. Computations for SRO are performed at temperatures slightly above the calculated order-disorder transition temperature T_c and also at high T (several hundred degrees above T_c). These SRO calculations provide a measure for the spatial correlations in Ni-V and Pd-V alloys, and *in some simple cases* (Table I) give the wave vectors of the underlying LRO states.

III. RESULTS: SRO OF Ni$_{1-x}$V$_x$ AND Pd$_{1-x}$V$_x$

The SRO patterns calculated using both $J_f(T = 0)$ and $J_f(T)$ for Ni$_{1-x}$V$_x$ and Pd$_{1-x}$V$_x$ alloys are shown in Figs. 2–5. These results are summarized in Table II, which gives the wave vectors $\mathbf{k}_{SRO}$ that produce peaks in the calculated $\alpha_{SRO}(x, \mathbf{k})$ as well as the dominant wave vectors $\mathbf{k}_{LRO}$ of the low-T LRO state. The calculated SRO wave vectors are compared with those of diffuse scattering experiments, where available.

Recently, Johnson *et al.*[30] performed local-density-approximation-based calculations (LDA) of the SRO of Ni$_{0.75}$V$_{0.25}$, Ni$_{0.67}$V$_{0.33}$, and Pd$_{0.75}$V$_{0.25}$ using a concentration-wave extension of the coherent-potential approximation. These authors found (i) $\mathbf{k}_{SRO} = \langle 1\frac{1}{2}0 \rangle$ and $\langle 100 \rangle$ for Ni$_{0.75}$V$_{0.25}$ and Pd$_{0.75}$V$_{0.25}$, respectively, in qualitative agreement with both the present calculations and the neutron scattering results of Caudron *et al.*[20] (ii) However, Johnson *et al.* found $\mathbf{k}_{SRO} = \langle 100 \rangle$ for Ni$_{0.67}$V$_{0.33}$, in qualitative conflict with our results (Fig. 3) and those of the experiment,[20] which both give $\mathbf{k}_{SRO} = \langle 1\frac{1}{2}0 \rangle$.

A. Effects of composition on LRO and SRO: Ni$_{1-x}$V$_x$

The Monte Carlo calculated $\alpha_{SRO}(\mathbf{k})$ is shown in the $(hk0)$ plane for Ni$_{1-x}$V$_x$ alloys in Figs. 2 and 3 using T-
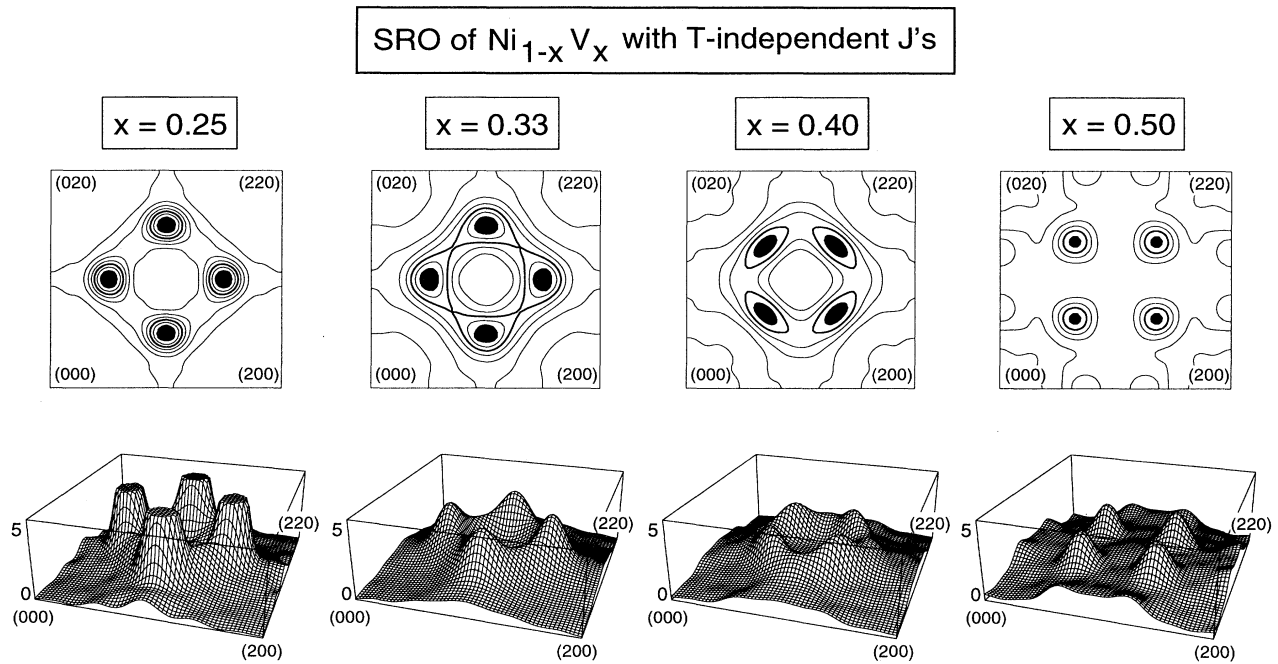
FIG. 2. Monte Carlo simulated annealing calculated values of $\alpha_{SRO}(\mathbf{k})$ for $Ni_{1-x}V_x$ alloys in the $(hk0)$ plane. The calculations were performed using T-independent J_f's derived from first-principles total energies. The black shading in the contour plots locates the peaks in the SRO pattern. The calculations for $x = 0.25$, 0.33, 0.40, and 0.50 were performed at 2300, 2250, 1700, and 1400 K, respectively. Contours are all spaced by 0.5, except for $x = 0.25$, in which contours are 1.0 apart.
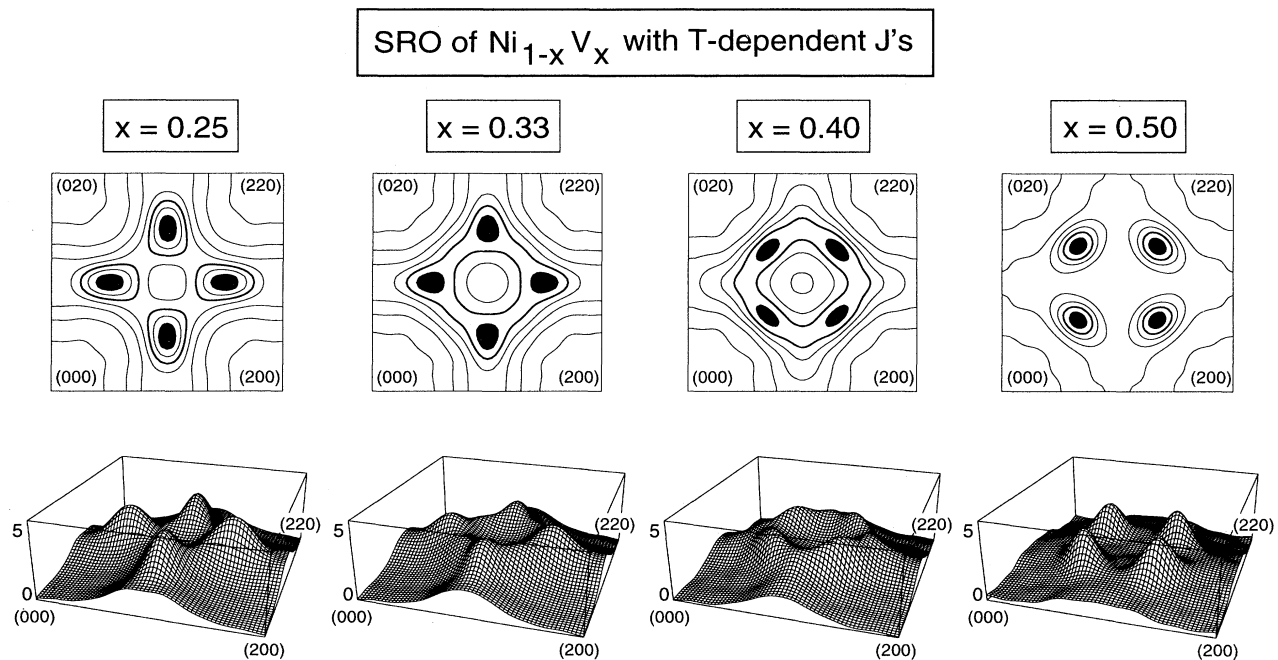
FIG. 3. Same as Fig. 2, except with T-dependent J_f's. The calculations for $x = 0.25$, 0.33, 0.40, and 0.50 were performed at 1700, 1875, 1900, and 1600 K, respectively. Contours are all spaced by 0.5.
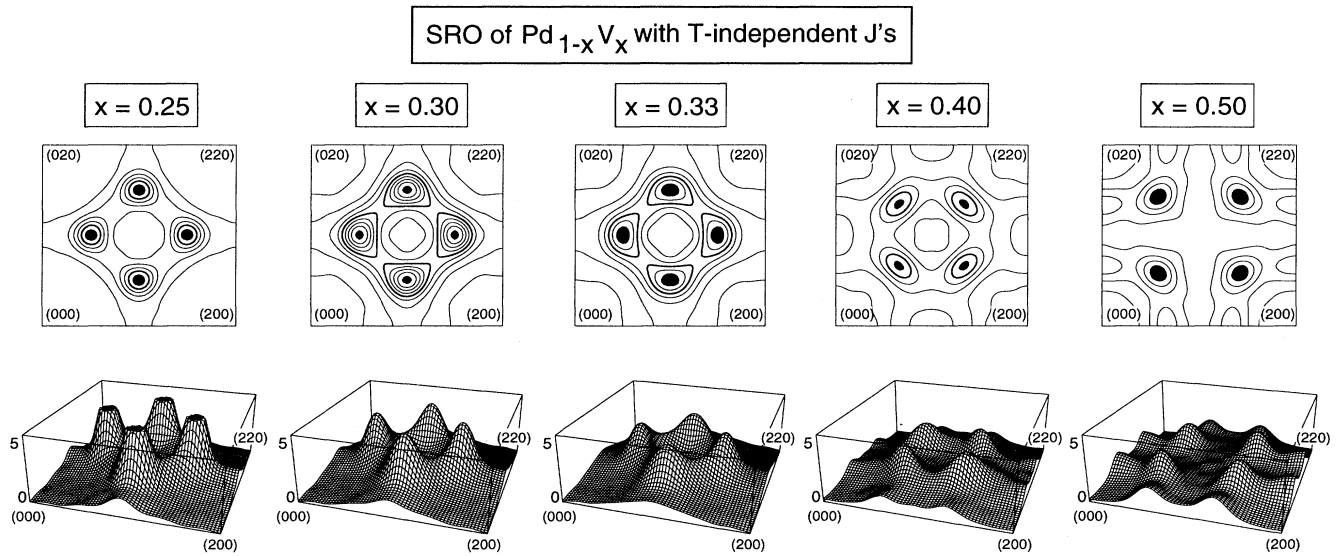
FIG. 4. Monte Carlo simulated annealing calculated values of $\alpha_{SRO}(\mathbf{k})$ for $Pd_{1-x}V_x$ alloys in the $(hk0)$ plane. The calculations were performed using T-independent J_f's derived from first-principles total energies. The black shading in the contour plots locates the peaks in the SRO pattern. The calculations for $x = 0.25, 0.30, 0.33, 0.40$, and 0.50 were performed at 1800, 1300, 1500, 1200, and 1150 K, respectively. Contours are all spaced by 0.5, except for $x = 0.25$, in which contours are 1.0 apart.

independent and T-dependent J_f's, respectively. Specifically, $\alpha_{SRO}(x, \mathbf{k})$ is shown for $x = 0.25, 0.33, 0.40$, and 0.50.[31]

For $x=0.25$, as shown previously,[28] the T-dependent J_f's serve to quantitatively reduce the peak intensity at the $\langle 1\frac{1}{2}0 \rangle$ points in $Ni_{0.75}V_{0.25}$, thereby bringing the calculations much closer to the diffuse intensity due to SRO observed by neutron diffraction.[20] The calculated ground state LRO of $Ni_{0.75}V_{0.25}$ is the $D0_{22}$ structure, $(\mathbf{k}_{LRO} = \langle 1\frac{1}{2}0 \rangle)$, in agreement with the experimentally

well-established phase diagram.[32] Thus, for Ni_3V, we have $\mathbf{k}_{SRO} = \mathbf{k}_{LRO}$ [Case $(iii)_a$ from Table I].

$Ni_{0.67}V_{0.33}$ shows peaks at $\mathbf{k}_{SRO} = \langle 1\frac{1}{2}0 \rangle$, in agreement with experimental measurements,[20] but in conflict with recent[30] first-principles calculations based on the coherent-potential approximation, which show peaks at the $\langle 100 \rangle$ points. Ni_2V in the $MoPt_2$ structure $(\mathbf{k}_{LRO} = \frac{2}{3}\langle 110 \rangle)$ is the predicted ground state of the calculations, in agreement with experimental observations.[32] Thus,
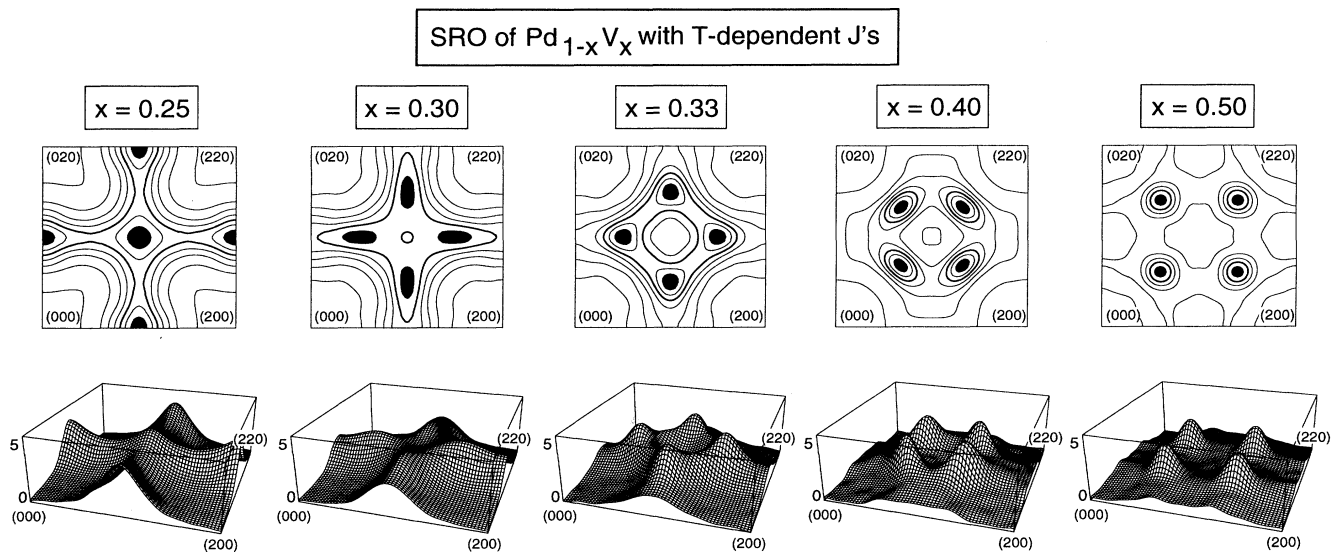
FIG. 5. Same as Fig. 4, except with T-dependent J_f's. The calculations for $x = 0.25, 0.30, 0.33, 0.40$, and 0.50 were performed at 1550, 1500, 1400, 1300, and 1300 K, respectively. Contours are all spaced by 0.5.

TABLE II. Dominant wave vectors of long- and short-range order in fcc-based Ni-V and Pd-V alloys. "Case/type" refers to the classification of Table I. $J_f(T)$ denotes temperature-dependent J_f's, while $J_f(0)$ denotes temperature-independent J_f's.

Alloy	$\mathbf{k}_{LRO}^{calc}$ $J_f(0)$ $T=0$ K	$\mathbf{k}_{LRO}^{expt\ a}$ $T < T_c$	$\mathbf{k}_{SRO}^{calc}$ $J_f(0)$ $T \gtrsim T_c$	$\mathbf{k}_{SRO}^{expt\ b}$ $T \gtrsim T_c$	$\mathbf{k}_{SRO}^{calc}$ $J_f(T)$ $T \gtrsim T_c$	$\mathbf{k}_{SRO}^{calc}$ $J_f(T)$ High T	Case/type
$Ni_{0.75}V_{0.25}$	$\langle 1\frac{1}{2}0\rangle$	$\langle 1\frac{1}{2}0\rangle$	$\langle 1\frac{1}{2}0\rangle$	$\langle 1\frac{1}{2}0\rangle$	$\langle 1\frac{1}{2}0\rangle$	$\langle 100\rangle$	(iii)$_a$
$Ni_{0.67}V_{0.33}$	$\frac{2}{3}\langle 110\rangle$	$\frac{2}{3}\langle 110\rangle$	$\langle 1\frac{1}{2}0\rangle$	$\langle 1\frac{1}{2}0\rangle$	$\langle 1\frac{1}{2}0\rangle$	$\langle 100\rangle$	(iv)$_c$
$Ni_{0.60}V_{0.40}$			$\langle \zeta\zeta0\rangle$		$\langle \zeta\zeta0\rangle$		
$Ni_{0.50}V_{0.50}$			$\langle \zeta\zeta0\rangle$		$\langle \zeta\zeta0\rangle$		(iv)$_b$
$Pd_{0.75}V_{0.25}$	$\langle 1\frac{1}{2}0\rangle$	$\langle 1\frac{1}{2}0\rangle$	$\langle 1\frac{1}{2}0\rangle$	$\langle 100\rangle$	$\langle 100\rangle$	$\langle 100\rangle$	(iv)$_a$
$Pd_{0.70}V_{0.30}$			$\langle 1\frac{1}{2}0\rangle$		$\langle 1\frac{1}{2}0\rangle$	$\langle 100\rangle$	
$Pd_{0.67}V_{0.33}$	$\frac{2}{3}\langle 110\rangle$	$\frac{2}{3}\langle 110\rangle$	$\langle 1\frac{1}{2}0\rangle$		$\langle 1\frac{1}{2}0\rangle$	$\langle 1\frac{1}{2}0\rangle,\langle 100\rangle$	(iv)$_c$
$Pd_{0.60}V_{0.40}$			$\langle \zeta\zeta0\rangle$		$\langle \zeta\zeta0\rangle$		
$Pd_{0.50}V_{0.50}$			$\langle \zeta\zeta0\rangle$		$\langle \zeta\zeta0\rangle$		(iv)$_b$

[a]See Ref. 32.
[b]See Refs. 20 and 22.

$Ni_{0.67}V_{0.33}$ corresponds to a case (iv)$_c$ alloy (Table I).

As x is increased to 0.40 and 0.50, the SRO peaks show a shift to non-special-points along the $\langle \zeta\zeta0\rangle$ line, near (but not precisely at) $\zeta = \frac{2}{3}$. (The dominant wave vector of the Ni$_2$V structure is $\mathbf{k}_{LRO} = \frac{2}{3}\langle 110\rangle$.) The experimentally observed LRO (Ref. 32) at $Ni_{0.5}V_{0.5}$ composition is a two-phase mixture of Ni$_2$V and an off-stoichiometric, V-rich σ phase (isostructural with σCrFe). In this paper, we deal only with fcc-based phases, and thus the σ phase is not amenable to our LRO calculations. Our simulated annealing calculation shows a LRO state at $x=0.5$ with a complex structure, nearly degenerate in energy with the $L1_0$ structure.

B. Effects of composition on LRO and SRO: $Pd_{1-x}V_x$

The Monte Carlo calculated $\alpha_{SRO}(\mathbf{k})$ is shown in the $(hk0)$ plane for $Pd_{1-x}V_x$ alloys in Figs. 4 and 5 using T-independent and T-dependent J_f's, respectively. Calculations are shown for $x = 0.25, 0.30, 0.33, 0.40$, and 0.50.[31]

For $x=0.25$ as was recently shown,[28] only when a T dependence is included in the J_f's, does one obtain $\mathbf{k}_{SRO} = \langle 100\rangle$, in agreement with the SRO observed from neutron diffraction experiments.[33] However, although the SRO peaks at the $\langle 100\rangle$ points, the predicted and observed[32] ground state is the $\langle 1\frac{1}{2}0\rangle$ DO_{22} structure. Thus, although both the LRO and SRO of $Pd_{0.75}V_{0.25}$ peak at special points in the Brillouin zone ($\langle 1\frac{1}{2}0\rangle$ and $\langle 100\rangle$, respectively), these wave vectors do not coincide, thus putting this alloy in case (iv)$_a$ of Table I.

For $x \neq 0.25$, calculations (Figs. 4 and 5) show $\mathbf{k}_{SRO} = \langle 1\frac{1}{2}0\rangle$ for $Pd_{0.67}V_{0.33}$. No experimental measurements of SRO exist for this composition (Caudron et al.[20] attempted to measure the SRO of $Pd_{0.67}V_{0.33}$, but reported difficulties in growing single crystals of the material), thus the shift of SRO from $\langle 100\rangle$ to $\langle 1\frac{1}{2}0\rangle$ as one goes from $x = 0.25$ to 0.33 represents a prediction of the present work. The simulated annealing calculation of LRO for Pd$_2$V using $J_f(T)$ shows LRO of the MoPt$_2$ type, in agreement with the observed Pd$_2$V structure.[32] When using $J_f(T = 0)$, however, the simulated annealing algorithm converges to a structure that is degenerate (within 1 meV/atom) with the MoPt$_2$ type, but is nonetheless a distinct ordered state. Both structures have $\mathbf{k}_{LRO} = \frac{2}{3}\langle 110\rangle$, as does the observed Pd$_2$V structure.[32] Thus, $Pd_{0.67}V_{0.33}$ is a case (iv)$_c$ alloy (Table I).

For $x > 0.33$, the SRO peaks of $Pd_{1-x}V_x$ show the same shift as did $Ni_{1-x}V_x$ to non-special-points along the $\langle \zeta\zeta0\rangle$ line, near $\frac{2}{3}\langle 110\rangle$. The assessed Pd-V phase diagram[32] shows no stable low-temperature phase at $Pd_{0.50}V_{0.50}$ composition, but rather shows fcc solid solution extending down to low temperature (~700 K). Our simulated annealing calculation for $Pd_{0.50}V_{0.50}$ shows a LRO state with a complex structure, nearly degenerate in energy with the $L1_0$ structure.

C. Calculations using T-independent J_f's: Summary of discrepancies with experiment

Using our calculational scheme (approach I, Fig. 1), we find several results using T-independent J_f's, which are unsatisfactory. We next summarize these discrepancies between experimental measurements and our calculations using $J_f(T = 0)$. We will then discuss the T dependence introduced into $J_f(T)$ in order to rectify these disagreements.

(i) The SRO of Pd$_3$V calculated using $J_f(T = 0)$ shows (Fig. 4) $\mathbf{k}_{SRO} = \langle 1\frac{1}{2}0\rangle$ points, whereas experimentally[20] it is seen to be $\langle 100\rangle$.

(ii) Measured diffuse scattering at high temperatures has been used to deduce[20,22] via approach II (Fig. 1), J_f's that should be capable of describing the energy of any configuration (i.e., not just the equilibrium state) at the temperature of the experiment. Using these J_f's in a cluster expansion, Caudron et al.[20] have recalculated the values of the energy difference between the perfectly ordered $L1_2$ and DO_{22} structures (depicted in Fig. 6), which we may compare with our first-principles calculated val-

$L1_2$ DO_{22}

1st A: 8A+4B	1st A: 8A+4B, 8A+4B
1st B: 12A+0B	1st B: 12A+0B
2nd A: 6A+0B	2nd A: 6A+0B, 4A+2B
2nd B: 0A+6B	2nd B: 2A+4B
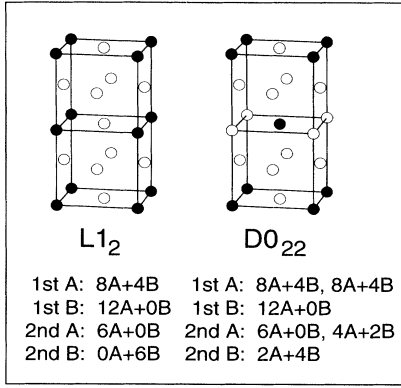
FIG. 6. The A_3B structures, $L1_2$ and DO_{22}. The unit cells of the two structures are shown as are the first- and second-neighbor coordinations for A and B atoms. Note that the two structures have indistinguishable nearest-neighbor environments, but distinct second-neighbor environments.

ues. The "experimentally inferred" values[20,22] (appropriate to high T) of the energy differences between $L1_2$ and DO_{22} for Ni_3V and Pd_3V have the same sign, but are considerably smaller ($+12 \pm 5$ and $+2.4 \pm 0.3$ meV/atom, respectively) than the corresponding LDA values ($+105$ and $+70$ meV/atom) calculated[28,34] at $T=0$ K.

(iii) Using our approach-I-type methodology, we have calculated transition temperatures (Table III) for Ni-V and Pd-V alloys. The calculated values using $J_f(T = 0)$ are $T_c = 1900$ K and 1600 K for Ni_3V and Pd_3V, respectively. These values are much too high when compared with those obtained from the experimental phase diagrams (1318 K and 1088 K, respectively).[32]

From problem (ii) above, we conclude that there must be some excitation that modifies the energies of the $L1_2$ and DO_{22} configurations such that the energy difference between these two structures is much smaller at high T than at low (or zero) T. *Configurational* excitations (e.g., long- or short-range order) cannot resolve the disparity between the high- and low-T energy differences because both experiment and calculation determine the energy difference between two *perfectly ordered* (i.e., not partially ordered) compounds. Thus, there must be a significant excitation in these alloys which is nonconfigurational in nature and which modifies the energies of the $L1_2$ and DO_{22} structures at finite temperatures. Thus, the temperature-dependent *free energy* difference between the perfectly ordered $L1_2$ and DO_{22} configura-

TABLE III. Calculated (Monte Carlo simulated annealing) and experimental (Ref. 32) order-disorder transition temperatures T_c (in Kelvin) for Ni-V and Pd-V alloys.

	T_c^{calc} T-indep. J's	T_c^{calc} T-dep. J's	T_c^{expt}
Ni_3V	1900	1400	1318
Ni_2V	1850	1750	1195
Pd_3V	1600	1250	1088
Pd_2V	1050	1200	1178

tions may be written as

$$\Delta F(T) \equiv F(L1_2) - F(DO_{22})$$
$$= \Delta E(T = 0) + \Delta E_{\text{excit}}(T) - T\Delta S_{\text{excit}}(T) . \quad (4)$$

The first term on the right-hand side of Eq. (4), $\Delta E(T = 0) \equiv E(L1_2) - E(DO_{22})$, is the total internal energy difference between $L1_2$ and DO_{22} at zero temperature. This term can be calculated by spin-polarized or non-spin-polarized LDA calculations, as appropriate. The quantities $\Delta E_{\text{excit}}(T)$ and $\Delta S_{\text{excit}}(T)$ refer to the energy and entropy differences associated with *nonconfigurational* excitations, which give a temperature dependence to the free energy difference $\Delta F(T)$. Examination of the density of states (DOS) at the Fermi energy $n(\epsilon_F)$ of the $L1_2$ and DO_{22} structures (Figs. 7 and 8) shows that the former has a much higher $n(\epsilon_F)$. This suggests that the energy of thermal excitations associated with electron-hole excitation across the Fermi surface [$\Delta E_{\text{el}}(T)$ and $\Delta S_{\text{el}}(T)$] is much lower in $L1_2$ than in DO_{22}. Hence, we next explore the contribution of electron-hole excitations to $\Delta E_{\text{excit}}(T)$ and $\Delta S_{\text{excit}}(T)$. Subsequently, we will examine the combination of spin-polarization and electron-hole excitations.

IV. ELECTRONIC EXCITATIONS IN Ni_3V AND Pd_3V

Consider the energy and entropy associated with electronic excitations, i.e., the temperature-dependent free energy associated with the Fermi-Dirac distribution $f(\epsilon, T)$. There are three different levels of approximation (1, 2, and 3; in decreasing order of accuracy) by which the energy and entropy associated with electronic excitations (E_{el} and S_{el}) may be determined from first-principles (e.g., self-consistent LDA) electronic structure calculations. In all cases, we consider the thermal population effects in a *static*, nonvibrating lattice.

A. Level 1

In this level, the temperature dependence of the Fermi-Dirac distribution is included in the self-consistency loop of the LDA calculation (in the case of this paper, LAPW). The charge density is computed by summing the square of the one-electron wave functions, weighted by the Fermi factor

$$\rho(\mathbf{r}, T) = \sum_i f(\epsilon, T)|\Psi_i|^2 , \quad (5)$$

where the sum is over all states i. Because the charge density and potential (and hence, the eigenvalues) must be determined self-consistently, the T dependence of the charge density leads to an explicit T dependence of the DOS, $n(\epsilon, T)$. The Fermi level $\mu(T)$ is then determined by the following condition:[35]

$$\int_{-\infty}^{+\infty} n(\epsilon, T) f(\epsilon, T) d\epsilon = N_{\text{tot}} , \quad (6)$$
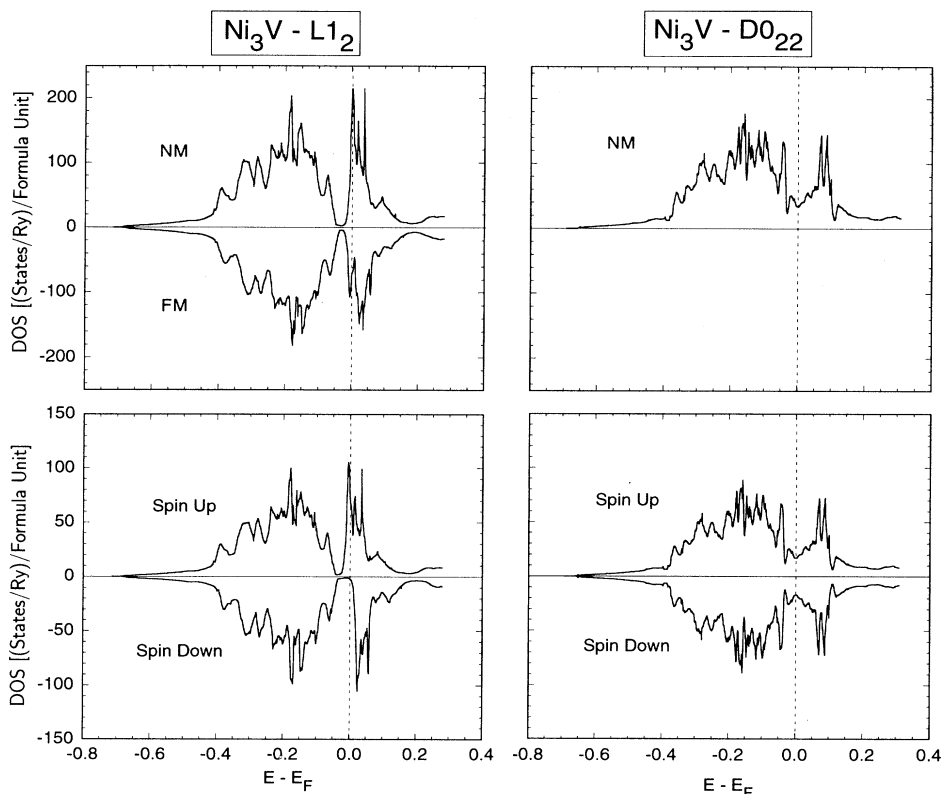
FIG. 7. LAPW calculated DOS for Ni_3V in the $D0_{22}$ and $L1_2$ structures. Shown are both nonmagnetic (NM) and ferromagnetic (FM) calculations. (Note that the FM calculation for the $D0_{22}$ structure converged to the NM solution.) The vertical dotted lines indicate the calculated Fermi level. The calculations shown are for $k_BT = 2$ mRy ($T = 316$ K).
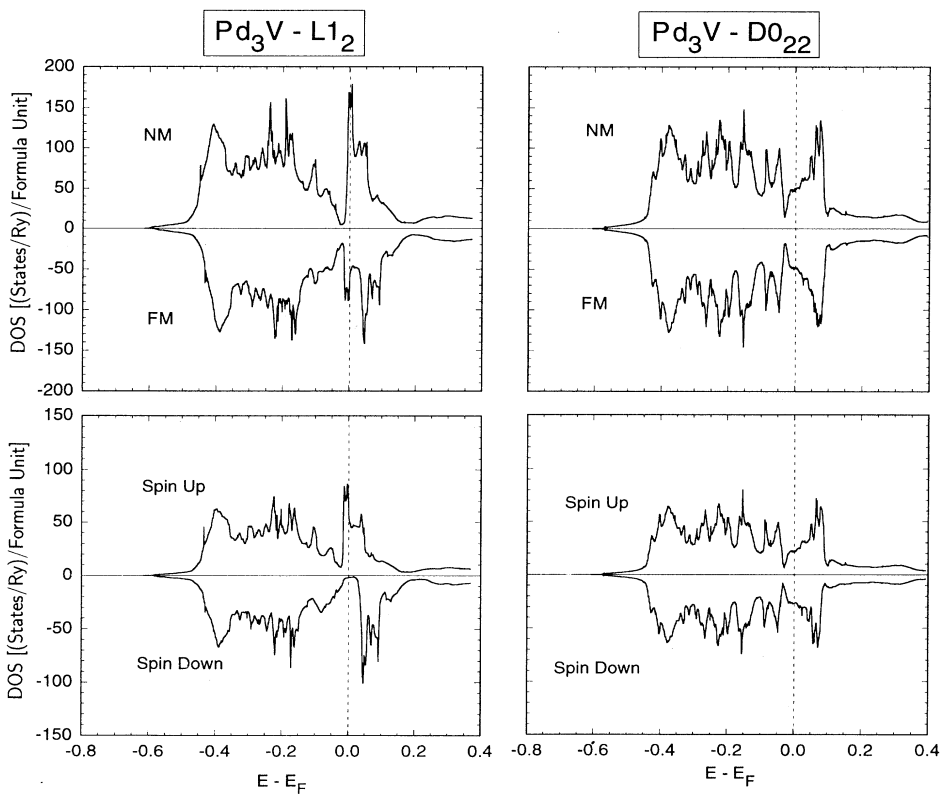
FIG. 8. LAPW calculated DOS for Pd_3V in the $D0_{22}$ and $L1_2$ structures. Shown are both nonmagnetic (NM) and ferromagnetic (FM) calculations. The vertical dotted lines indicate the calculated Fermi level. The calculations shown are for $k_BT = 2$ mRy ($T = 316$ K).

where N_{tot} is the total number of valence electrons. Once $n(\epsilon, T)$ and $\mu(T)$ are determined for a given temperature, the entropy due to electronic excitations[36] may be computed from the integral

$$S_{\text{el}}^{(1)}(T) = -\int_{-\infty}^{+\infty} n(\epsilon, T)\{f(\epsilon, T)\ln f(\epsilon, T)$$
$$+[1 - f(\epsilon, T)]\ln[1 - f(\epsilon, T)]\} \, d\epsilon. \qquad (7)$$

The entropy $S_{\text{el}}^{(1)}$ in Eq. (7) has a temperature dependence due to (i) the explicit and implicit [due to the $\mu(T)$] T dependence of the Fermi distribution, and (ii) the T-dependent DOS. The contribution of electronic excitations to the *internal energy* is given by the difference between the $T = 0$ total energy from LDA, and that calculated at finite temperature by using the Fermi distribution in evaluating the charge density and sums of eigenvalues. The total-energy expression is given by

$$E_{\text{tot}}(T) = \sum_i f(\epsilon, T) \, \epsilon_i + \tilde{E}[\rho(\mathbf{r}, T)]$$
$$+\frac{1}{2} \sum_{\alpha,\beta} \frac{Z_\alpha Z_\beta}{|\mathbf{R}_\alpha - \mathbf{R}_\beta|} \,, \qquad (8)$$

where the third term is the T-independent ion-ion Coulomb energy and the second term $\tilde{E}[\rho(\mathbf{r}, T)]$ is a functional of the charge density

$$\tilde{E}[\rho(\mathbf{r}, T)] = -\frac{1}{2} \int \int \frac{\rho(\mathbf{r}, T)\rho(\mathbf{r}', T)}{|\mathbf{r} - \mathbf{r}'|} \, d^3\mathbf{r} \, d^3\mathbf{r}'$$
$$+E_{\text{xc}}[\rho(\mathbf{r}, T)]$$
$$-\int \rho(\mathbf{r}, T)V_{\text{xc}}[\rho(\mathbf{r}, T)] \, d^3\mathbf{r} \,. \qquad (9)$$

The terms in Eq. (9) are the electron-electron Coulomb energy, the exchange-correlation energy, and the term involving the exchange-correlation potential, V_{xc}. In level 1 then, the energy due to electronic excitations is not merely given by the sum of one-electron eigenvalues, but rather due to self-consistency, is truly a difference of *total* energies:

$$E_{\text{el}}^{(1)}(T) = E_{\text{tot}}(T) - E_{\text{tot}}(T = 0) \,. \qquad (10)$$

The total free energy change due to electronic excitations is given by Eqs. (7) and (10) as $F_{\text{el}}^{(1)}(T) = E_{\text{el}}^{(1)}(T) - TS_{\text{el}}^{(1)}(T)$. In the self-consistency loop of the LDA calculations, the potential used is the functional derivative of the *internal* energy with respect to charge density, $\partial E[\rho]/\partial\rho$, (rather than the correct expression, $\partial F[\rho]/\partial\rho$) and hence minimizes $E_{\text{tot}}(T)$. Once self-consistency is achieved, the entropy of Eq. (7) is computed and $-TS_{\text{el}}$ is added to E_{tot}. For the alloys considered here, we expect this approximation to introduce only small errors in $F_{\text{el}}(T)$. A level 1 approach has recently been used to determine the free energy of electronic excitations in pure Cu in the context of multiple-scattering calculations.[37]

B. Level 2

Here it is assumed that the DOS has no explicit temperature dependence, and therefore, the entropy is given

by Eq. (7) using the $T = 0$ DOS:

$$S_{\text{el}}^{(2)}(T) = -\int_{-\infty}^{+\infty} n(\epsilon, T = 0)\{f(\epsilon, T)\ln f(\epsilon, T)$$
$$+[1 - f(\epsilon, T)]\ln[1 - f(\epsilon, T)]\}d\epsilon. \qquad (11)$$

Thus, in the level 2 approximation, S_{el} is given a temperature dependence only through the Fermi distribution. This approximation has been used to determine the electronic entropy of several pure transition metals in Ref. 36. The energy E_{el} in level 2 is given by only one-electron terms, i.e., from integrating the $T = 0$ DOS:

$$E_{\text{el}}^{(2)} = \int_{-\infty}^{+\infty} \epsilon \, n(\epsilon, T = 0) \, f(\epsilon, T) \, d\epsilon$$
$$-\int_{-\infty}^{\epsilon_F} \epsilon \, n(\epsilon, T = 0) \, d\epsilon \,. \qquad (12)$$

The free energy of electronic excitations in level 2 is $F_{\text{el}}^{(2)}(T) = E_{\text{el}}^{(2)}(T) - TS_{\text{el}}^{(2)}(T)$.

C. Level 3 (Sommerfeld approximation)

Here, one assumes not only that the density of states is temperature independent, but also that the density of states near the Fermi energy varies slowly with ϵ, and that the electron states are probed in a sufficiently narrow range (at a sufficiently low temperature) about the Fermi level such that the DOS is roughly constant and may be taken outside the integrals of Eqs. (11) and (12) as the constant, $n(\epsilon_F)$. The resulting energy associated with electronic excitations is given by

$$E_{\text{el}}^{(3)} = \frac{\pi^2}{6} k_B^2 T^2 n(\epsilon_F) \qquad (13)$$

and the entropy expression is

$$S_{\text{el}}^{(3)} = \frac{\pi^2}{3} k_B^2 T n(\epsilon_F) \,. \qquad (14)$$

Equations (13) and (14) are commonly referred to as the Sommerfeld model (to lowest order in temperature) for electronic excitations.[38] The free energy of electronic excitations in the Sommerfeld model (level 3) is quadratic in temperature:

$$F_{\text{el}}^{(3)}(T) = E_{\text{el}}^{(3)}(T) - TS_{\text{el}}^{(3)}(T) = AT^2 \,, \qquad (15)$$

where the constant $A = -\frac{\pi^2}{6} k_B^2 n(\epsilon_F)$. In the Sommerfeld model, not only is the DOS at the Fermi level assumed to be a constant, independent of temperature, but implicitly, the Sommerfeld approach also of Eqs. (13) and (14) assumes that (to lowest order), the Fermi level is relatively temperature independent. It is evident from Eqs. (13) and (14) that *electronic excitations contribute to the relative stability of two equal-composition structures only for the rare case when the DOS of these structures at ϵ_F is significantly different.*

D. Phenomenological fitting

Motivated by Eq. (15) one may model the temperature-dependent free energy difference between

the $L1_2$ and $D0_{22}$ structures [Eq. (4)] with a quadratic temperature dependence

$$\Delta F(T) = \Delta E(T = 0) - AT^2 , \qquad (16)$$

where A is a constant. In a previous paper,[28] we used Eq. (16) in our calculations of SRO in Ni_3V and Pd_3V by mapping a quadratic T dependence onto a three- and four-body interaction, J_3 and K_4, respectively.[39] In the spirit of a model calculation, we adjusted the constant A in Eq. (16) so as to bring the calculated SRO of Ni_3V and Pd_3V in agreement with neutron diffuse scattering measurements. The values of A $(= A_{fit})$ that *reproduce* the observed SRO patterns in Ni_3V and Pd_3V [$A_{fit} = -54.4$ and -50.1 ($Ry^{-1}atom^{-1}$), respectively] are used here in Figs. 3 and 5 for all compositions. The T dependence of the J_f's leads not only to calculated SRO, which is in excellent quantitative agreement with experiment, but also significantly reduces the transition temperatures (Table III), thereby bringing them much closer to experiment. Thus, the T-dependent J_f's are clearly more accurate in describing the LRO and SRO of Ni-V and Pd-V alloys than their T-independent counterparts. Using $J_f(T)$, we have also calculated the SRO at high T. The wave vectors of these high-T SRO patterns are given in Table II. In several cases, the high-T limit of the SRO shows a shift of peak wave vector. For example, in $Ni_{0.75}V_{0.25}$ and $Ni_{0.67}V_{0.33}$, the calculated k_{SRO} shifts from $\langle 1\frac{1}{2}0 \rangle$ to $\langle 100 \rangle$ as temperature is increased. This shift of k_{SRO} in $Ni_{0.75}V_{0.25}$ has also been predicted by previous first-principles calculations.[28,30]

E. First-principles calculation of electronic excitations

We now examine the accuracy of the Sommerfeld model (level 3) with respect to levels 1 and 2. This comparison will quantitatively determine to what extent the phenomenologically fitted T dependence of $\Delta F(T)$ [Eq. (16)] is due to electronic excitations as described by no-phonon band theory. Using first-principles full-potential LAPW[40] calculations of Ni_3V and Pd_3V in the fully relaxed $D0_{22}$ and $L1_2$ structures, we have computed the DOS and total energies as explicit functions of temperature. In the LAPW calculations, we have used the exchange correlation of Ceperley and Alder,[41] as parametrized by Perdew and Zunger.[42] The muffin-tin radii are chosen to be 2.2 a.u. for Ni and 2.4 a.u. for Pd, and 2.3 (2.4) a.u. for V in the Ni_3V (Pd_3V) calculations. Brillouin-zone integrations are performed using the equivalent k-point sampling method.[43] We used 20 and 40 k points in the irreducible zone for the $L1_2$ and $D0_{22}$ structures, respectively, with both mapping onto to same 60 special k points[44] for the fcc structure. This mapping guarantees that the total energy per atom of an elemental metal calculated either with the fcc unit cell or with a lower symmetry ($L1_2$ or $D0_{22}$) are identical. All total energies are optimized with respect to volume as well as the c/a ratio in the $D0_{22}$ structure. Lattice constants were not reevaluated at each temperature, but rather the low-T calculated values were used for all tem-

peratures. The calculated lattice constants are $a = 3.48$ and 3.80 Å for Ni_3V and Pd_3V in the $L1_2$ structures, and a (c) = 3.45 (7.04) and 3.78 Å (7.62 Å) for the $D0_{22}$ structures. Our calculated values for the tetragonal distortion in $D0_{22}$ are $c/a = 2.040$ and 2.016 in Ni_3V and Pd_3V, which agree well with the experimental values[45] of 2.036–2.040 and 2.015.

In this section, we describe the results of non-spin-polarized calculations, and in the following section, we examine the corrections due to spin polarization on the DOS and the T dependence of $\Delta F(T)$. The calculated DOS are shown for Ni_3V and Pd_3V in Figs. 7 and 8, respectively, and illustrate that $n(\epsilon_F)$ is much larger in the $L1_2$ structures than in the $D0_{22}$ structures, for both Ni_3V and Pd_3V. The calculated DOS and total energies have also been used to determine $F_{el}^{(i)}$, $E_{el}^{(i)}$, and $S_{el}^{(i)}$ for all three levels $(i = 1, 2, 3)$ described above. The results for the Ni_3V and Pd_3V alloys are shown in Figs. 9 and 10, respectively. We note the following:

(i) In all non-spin-polarized cases considered, the temperature dependence of the DOS was found to be negligible; thus, in all cases level 2 provides an accurate approximation, as compared with level 1 as evidenced by the proximity of the solid lines (level 2) to the solid circles (level 1) in Figs. 9 and 10.

(ii) The Sommerfeld approximation (level 3) slightly underestimates the magnitude of E_{el} and S_{el} for Ni_3V and Pd_3V in the $D0_{22}$ structure, but *significantly over-estimates* E_{el} and S_{el} for these alloys in the $L1_2$ structure. The reason is that in the $L1_2$ structure, the DOS at the temperature-dependent *Fermi level* $\mu(T)$ is rapidly varying. At zero temperature $\mu(T = 0) = \epsilon_F$ falls near a sharp peak in the DOS (Figs. 7 and 8). However, $\mu(T)$ shifts towards lower energies with increasing T, coming close to the pseudogap region of the DOS, and hence at high T, $n[\mu(T)]$ is significantly reduced. For the $D0_{22}$ structure, ϵ_F falls in a slowly varying portion of the DOS, and thus, as the Fermi level moves with increasing temperature, $n[\mu(T)]$ is hardly affected, and the Sommerfeld model proves to be a much more accurate approximation.

(iii) Due to thermal expansion, the bandwidth of the DOS contracts as T is increased, and hence the DOS at the Fermi level should increase. Thus, thermal expansion leads to a slight *upward* curvature of S_{el}, opposed to the pronounced downward curvature seen in Figs. 9 and 10 for the $L1_2$ alloys. However, we find that this effect is negligible (for a 1% increase in lattice constant), and thus do not include it in our calculations.

(iv) It is possible to experimentally measure S_{el}.[36] For Ni_3V and Pd_3V in the $D0_{22}$ structure, the low-T electronic specific heat coefficient, has been measured[36(c)] and (in the low-T limit) may be related[38] to $n(\epsilon_F)$ by the expression: $\gamma = \frac{1}{3}\pi^2 k_B^2 n(\epsilon_F)(1 + \lambda)$, where λ is an electron-phonon enhancement factor. Using the first-principles values of $n(\epsilon_F)$ in this expression reproduces the experimental values of γ, for enhancements γ of the order of $\frac{1}{2}$.

By combining the results of Figs. 9 and 10 with the calculated LDA values of $\Delta E(T = 0)$, we show in Fig. 11 the T dependence of $\Delta F(T)$ due to electronic excitations. Figure 11 shows that electronic excitations do

lower the LDA values of $\Delta E(T = 0)$ at finite temperatures, thus better approaching the experimental results (diamond symbols). However, although the Sommerfeld model (level 3) agrees best with experiment, it gives much too large a reduction of $\Delta F(T)$ at finite temperatures relative to the physically more accurate level 1 or 2 calculations. From the experimental values of $\Delta F(T)$ for Ni_3V and Pd_3V measured at $T = 1373$ K and 1128 K, respectively, it is clear that (level 1) electronic excitations do not account for the entire difference between $\Delta E(T = 0)$ as computed from LDA and $\Delta F(T)$ at finite T (from diffuse scattering measurements). Rather, our non-spin-polarized calculations (levels 1 and 2) show that *electronic excitations are responsible for roughly 25% of the difference.* (Our calculations for levels 1 and 2 show that A_{LDA} are about 25% of A_{fit}.) Thus, the *physical* origin of the constant A in Eq. (16) is not purely electronic excitations.

F. Effects of spin polarization

Figures 7 and 8 demonstrated that the $L1_2$ structure has a much higher DOS at ϵ_F than the $D0_{22}$ structure. In the previous section we explored the consequences of this difference on thermal electronic excitations. Here we note that such a difference in DOS can also have a

magnetic consequence: spin polarization lowers the energy of a structure having a high $n(\epsilon_F)$. Thus, we next examine the effects of spin polarization on the DOS and T dependence of $\Delta F(T)$ for Ni_3V and Pd_3V. To this end, we have performed spin-polarized LAPW calculations of the $D0_{22}$ and $L1_2$ structures including electronic excitations in levels 1, 2, and 3 described above. Details of the spin-polarized calculations are identical to the non-spin-polarized case described in the previous section, with the obvious exception that the spin-polarized form of the exchange-correlation functional is used. All lattice constants were reoptimized for the spin-polarized calculations, and were found to be equal to those of non-spin-polarized calculations, with the exception of Ni_3V $L1_2$, which has a small lattice expansion upon spin-polarization, from $a = 3.48$ to 3.49 Å. All spin-polarized calculations were performed in ferromagnetic (FM) geometries, i.e., with the symmetry of the magnetic calculation being identical to the symmetry of the nonmagnetic (NM) calculation.

Figures 7 and 8 show the effect of spin polarization on the DOS of Ni_3V and Pd_3V, respectively. For the $D0_{22}$ structures, spin polarization has only a small effect on the DOS (Pd_3V) or none at all (Ni_3V). The corresponding local magnetic moments for the $D0_{22}$ structures are small ($\mu_B = 0.0$ and 0.2 for the V atoms in Ni_3V and
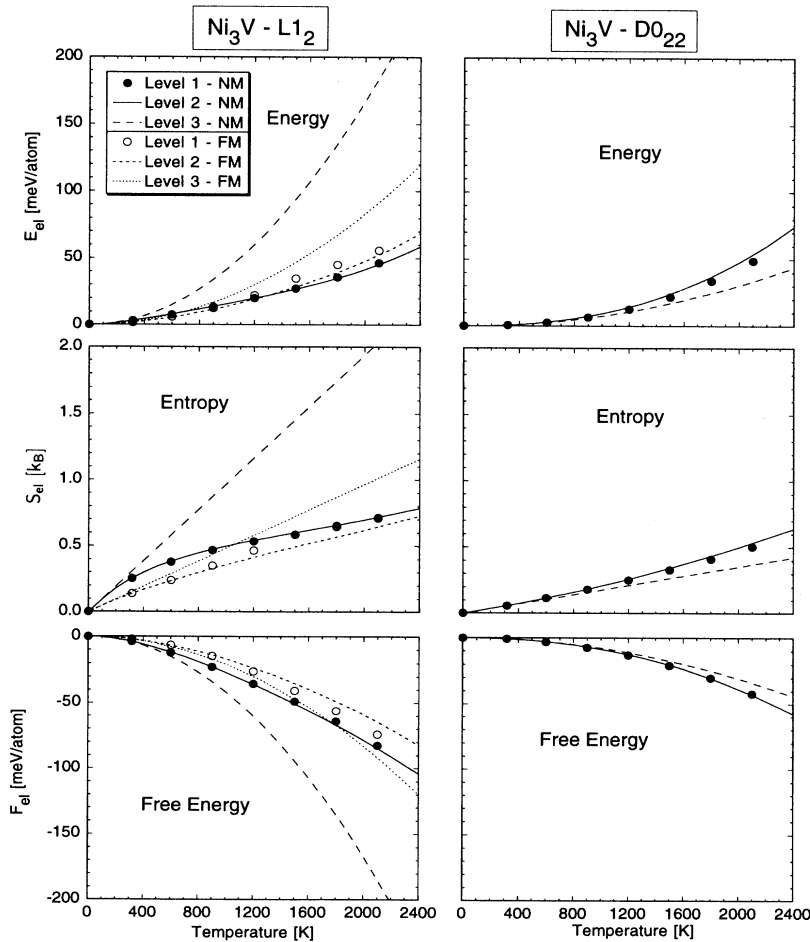
FIG. 9. Energy, entropy, and free energy associated with electronic excitations for Ni_3V in the $D0_{22}$ and $L1_2$ structures.

Pd$_3$V, respectively). *For the L1$_2$ structures, however, spin polarization splits the large peak in the DOS near* ϵ_F, *so that* $n(\epsilon_F)$ *is significantly reduced as compared with NM calculations.* This leads to larger magnetic moments on the V atoms in the L1$_2$ structures ($\mu_B = 0.8$ and 1.2 for Ni$_3$V and Pd$_3$V, respectively) than in the D0$_{22}$ structures. This reduction of $n(\epsilon_F)$ due to spin polarization has recently been shown to affect the D0$_{22}$/L1$_2$ structural stability in a large variety of Pd$_3$X($X = 3d$) compounds[46(a)] and has also been shown to qualitatively change the ordering tendency of Fe-Co alloys.[46(b)] Also, in contrast to all the NM calculations, the T dependence of the L1$_2$ DOS is not negligible for the spin-polarized calculations: At low T, the FM DOS is significantly distinct from the NM DOS; however, as T is increased, the FM calculations converge towards the NM solution (with no magnetic moments) and thus, the FM DOS evolves towards the NM DOS.

The effect of spin polarization on E_{el}, S_{el}, and F_{el} is illustrated in Figs. 9 and 10. Contrasting the most accurate (level 1) FM and NM calculations (open and filled circles), one can see that for L1$_2$ Ni$_3$V and Pd$_3$V, spin polarization reduces the magnitude of S_{el} and F_{el} relative to the NM calculations. This reduction is due to the lowering of $n(\epsilon)$ upon spin polarization. Note that spin polarization has a negligible effect on the electronic

excitations in the D0$_{22}$ structures. Also, as was the case for NM calculations, the FM level 3 calculations overestimate the effect of electronic excitations, but this overestimation is not as great as in the NM case [again, due to the spin-polarized reduction in $n(\epsilon_F)$]. Level 2 is fairly accurate compared with level 1 (as in the NM case); however, the T dependence of the FM DOS in the L1$_2$ structures leads to some inaccuracies in a FM level 2 approach.

Figure 11 illustrates the effects of spin polarization on the temperature-dependent free energy difference between the L1$_2$ and D0$_{22}$ structures $\Delta F(T)$ [Eq. (4)]. At low T, spin polarization of the L1$_2$ structure leads to a significant reduction in $\Delta F(T)$ in the direction of the experimental result. The energy lowering we find here due to spin polarization at $T=0$ is in excellent agreement with previous LAPW calculations for Pd$_3$V,[46] and is slightly smaller than that found by Lin *et al.*[34] for Ni$_3$V using LMTO calculations. The reduction of $\Delta F(T)$ (with respect to NM calculations) due to spin polarization becomes smaller with increasing temperature. For Ni$_3$V, the difference between FM and NM calculations becomes negligible at 900–1200 K. At T_c, the most accurate (level 1) FM calculations of $\Delta F(T_c)$ in Ni$_3$V and Pd$_3$V are reduced by $\sim$0 and 30% relative to the NM $\Delta F(T_c)$. However, these reductions due to the combination of electronic excitations and spin polarization ac-
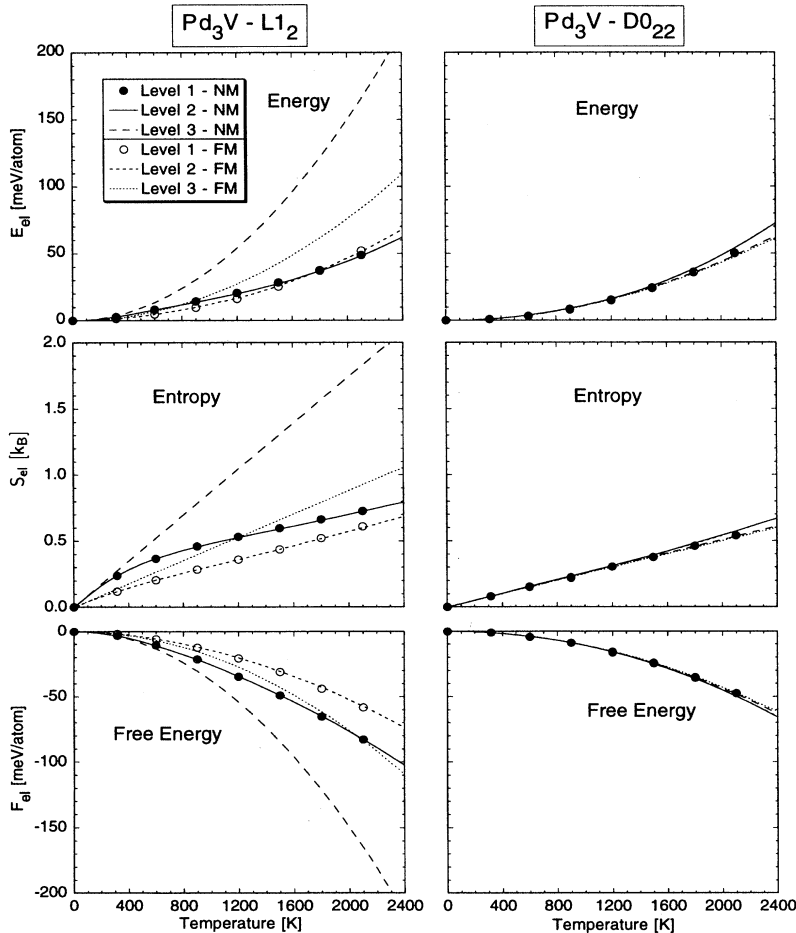
FIG. 10. Energy, entropy, and free energy associated with electronic excitations for Pd$_3$V in the D0$_{22}$ and L1$_2$ structures.

count for only ~ 30 and 50% of the discrepancy between $\Delta F(T)$ of experiment and that of LDA at $T=0$ in Ni_3V and Pd_3V, respectively.

Our results for the effects of electronic excitations (level 1) and spin polarization on $\Delta F(T)$ are summarized in Fig. 12. We see that the two nonconfigurational excitations are not additive: In Ni_3V, electronic excitations and spin polarization each independently reduce $\Delta F(T)$ by 27 and 8%, respectively. These percentages are 26 and 44% in Pd_3V. However, the combination of the two effects leads to reductions of 28 and 51% in Ni_3V and Pd_3V, significantly less than the sum of the two effects independently. Hence these effects do not fully account for the T dependence of the interactions used here (A_{fit}) to calculate SRO.

At present, we do not have a satisfactory explanation for the physical mechanism behind the fitted value of A. It is interesting to consider physical mechanisms other than electronic excitations or spin polarization, which could be responsible for the discrepancy between A_{fit} and A_{LDA}, i.e., for further lowering $\Delta F(T)$ at finite temperatures. One such excitation is that of lattice vibrations: If the vibrational free energy of the $L1_2$ and $D0_{22}$ structures are sufficiently different, they may also contribute

to a T dependence of $\Delta F(T)$. Also, electron-phonon or spin-orbit coupling could distinguish $L1_2$ from $D0_{22}$.

Johnson et al.[30] performed a non-spin-polarized level 2 LDA calculation[47] for the energy differences between $L1_2$ and $D0_{22}$ for Ni_3V and Pd_3V at finite T. These authors' calculations involved a concentration wave extension of the coherent potential approximation, implemented within the Korringa-Kohn-Rostoker multiple-scattering framework, as well as the following specifics: The atomic sphere approximation (ASA) was used with equal sphere sizes, the calculations were performed scalar relativistically, no charge correlations were included, and relaxation of the $D0_{22}$ structure was neglected. Johnson et al. found $\Delta F(T)$ values of -0.4 and -1.5 meV/atom for Ni_3V and Pd_3V at $T = 700$ and 850 K, respectively. These values are to be contrasted with our non-spin-polarized level 2 values at these temperatures: $+94$ and
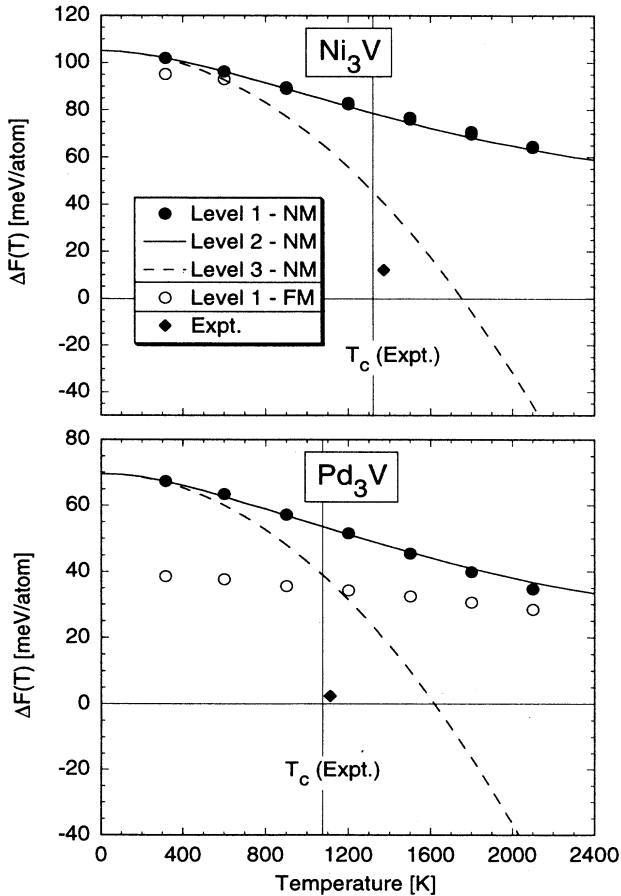
FIG. 11. LAPW calculated free energy differences due to electronic excitations between the $L1_2$ and $D0_{22}$ structures for Ni_3V and Pd_3V.
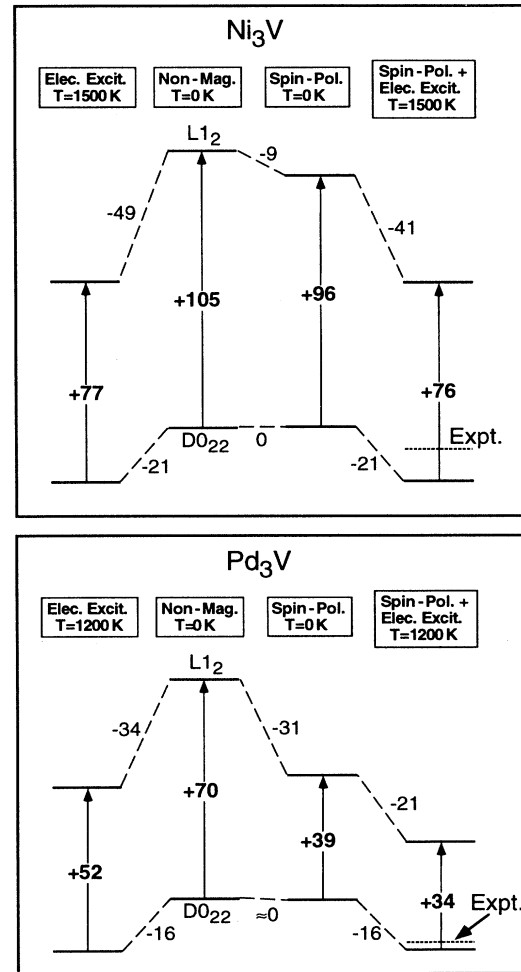
FIG. 12. Ni_3V and Pd_3V free energy differences (meV/atom) between the $L1_2$ and $D0_{22}$ structures due to electronic excitations, spin polarization, and a combination of the two effects. The dotted lines indicate the "experimentally inferred" values (Refs. 20 and 22) of $+12 \pm 5$ and $+2.4 \pm 0.3$ meV/atom for Ni_3V and Pd_3V, measured at $T = 1373$ K and 1128 K, respectively.

+58 meV/atom. Our calculations include charge correlations and are full potential, thus avoiding the ASA. An LDA-based theory, which includes F_{el} in a level 2 fashion should, at best, obtain a value of $\Delta F(T)$ at finite T, which is only *slightly reduced* compared to that of LDA at $T=0$, i.e., $\Delta E(T = 0)$ of $+105$ and $+70$ meV/atom [see Eq. (4)]. We therefore find the strong reduction of $\Delta E(T = 0) - \Delta F(T)$ that Johnson *et al.* found to be inexplicable.

V. CONCLUSIONS

We have studied the effects of composition and temperature on the SRO, electronic excitations, and spin polarization in $Ni_{1-x}V_x$ and $Pd_{1-x}V_x$ alloys. We find several compositions for which the dominant wave vectors of LRO and SRO do not coincide, and several shifts of the SRO peaks as a function of composition and temperature: (i) In $Ni_{0.75}V_{0.25}$, the SRO shows peaks at the $\langle 1\frac{1}{2}0 \rangle$ points near T_c, but this peaks shifts to the $\langle 100 \rangle$ points at high temperature. (ii) As x is increased from 0.33 to 0.40, the peak SRO of both $Ni_{1-x}V_x$ and $Pd_{1-x}V_x$ shifts from the special point $\langle 1\frac{1}{2}0 \rangle$ to a non-special-point along the $\langle \zeta\zeta0 \rangle$ line. (iii) The calculated [using $J_f(T)$] and observed SRO of Pd_3V peaks at the $\langle 100 \rangle$ points, even though the LRO at this composition is a $\langle 1\frac{1}{2}0 \rangle$-type structure. (iv) The SRO of $Pd_{1-x}V_x$ shifts from $\langle 100 \rangle \rightarrow \langle 1\frac{1}{2}0 \rangle \rightarrow \langle \zeta\zeta0 \rangle$, as x increases from $0.25 \rightarrow 0.33 \rightarrow 0.40$.

In Ni_3V and Pd_3V, first-principles calculations show that the DOS at the Fermi level is significantly higher in the $L1_2$ structure than in $D0_{22}$. This indicates that thermal electronic excitations could play an important role in the configurational energetics of these alloys at finite T. These excitations lead to an explicit temperature dependence of J_f, and we find that only when an explicit (phenomenologically fitted) temperature dependence of the J_f's is included do calculated SRO patterns and transition temperatures agree quantitatively with experiment. Configurational excitations do not manifest themselves as $J_f(T)$, thus, in these alloys some *nonconfigurational* excitation must be significant.

For Ni_3V and Pd_3V, discrepancies arise between total-energy differences of the $D0_{22}$ and $L1_2$ structures as determined from $T=0$ LDA calculations, and those energy differences deduced from diffuse scattering measurements. We have performed temperature-dependent self-consistent total-energy calculations (both spin polarized and non-spin-polarized) using a Fermi-Dirac distribution in evaluation of the charge density and Fermi level. In this way, we have calculated the energetic and entropic effects of electronic excitations on the $D0_{22}$ and $L1_2$ structures. We find in the non-spin-polarized case that electronic excitations are responsible for reducing the discrepancy between experiment and $T=0$ LDA by ~25%. The combination of spin polarization and electronic excitations reduces the discrepancy by ~30–50%. Thus, electronic excitations are not fully responsible for the discrepancy, and also are not the entire physical reason for the T dependence of the J_f's used in the SRO calculations. Some other nonconfigurational excitation (e.g., vibrational) must be responsible for further lowering $\Delta F(T)$ at finite temperatures.

[1] M. A. Krivoglaz and A. A. Smirnov, *The Theory of Order-Disorder in Alloys* (McDonald, London, 1964); P. C. Clapp and S. C. Moss, Phys. Rev. **142**, 418 (1966).

[2] The alternative form of Eq. (3),

$$\alpha_{SRO}(x, \mathbf{k}) = \frac{1}{1 + 4x(1 - x)[J_2(\mathbf{k}) - \Lambda]/kT}$$

with

$$\Lambda = \int d^3\mathbf{k}\, J_2(\mathbf{k})\, \alpha_{SRO}(x, \mathbf{k}),$$

has been used by J. B. Staunton, D. D. Johnson, and F. J. Pinski, Phys. Rev. B **50**, 1450 (1994); **50**, 1473 (1994). In a previous study [C. Wolverton and A. Zunger, Phys. Rev. B **51**, 6876 (1995)], we have found qualitatively very similar $\alpha_{SRO}(x, \mathbf{k})$ patterns using Eq. (3) or that of Staunton *et al.*

[3] The problem of finding the lowest-energy LRO states at zero temperature for a given $J_2(\mathbf{k})$ has been solved for cases involving a limited number of *real-space* pair interactions, $J_2(n)$. For a recent review, see F. Ducastelle, *Order and Phase Stability in Alloys* (Elsevier, New York, 1991).

[4] For alloys in which the LRO and SRO states are based on the same underlying parent lattice, cases in which the wave vectors of LRO and SRO are distinct may be grouped into (at least) three categories: (i) *Distinctions due to coherency*: In some alloys [e.g., Ni-Au, see Z.-W. Lu and A. Zunger, Phys. Rev. B **50**, 6626 (1994)], the ground-state LRO is *incoherent* phase separation, and all compounds have a positive formation enthalpy. However, if coherency is maintained, several compounds may have an energy lower than a *coherent* phase-separated state, and alloy SRO at high T is shown to exhibit ordering tendencies. (ii) *Distinctions due to geometry*: For example, the Ni_2V structure ($MoPt_2$ type) is characterized by $\mathbf{k}_{LRO} = \frac{2}{3}\langle 110 \rangle$, but the SRO at this composition peaks at the $\langle 1\frac{1}{2}0 \rangle$ points. It is impossible (simply due to geometry) to build an A_2B structure composed entirely of $\langle 1\frac{1}{2}0 \rangle$ waves. In fact [D. de Fontaine, Acta. Metall. **23**, 553 (1975)], the $MoPt_2$-type structure may be grouped into the $\langle 1\frac{1}{2}0 \rangle$ *family* of structures when one considers that the $\frac{2}{3}\langle 110 \rangle$ point (inside the first Brillouin zone) is equivalent to the $\frac{4}{3}\langle 1\frac{1}{2}0 \rangle$ point (out-

side the first Brillouin zone). (iii) *Distinctions due to non-mean-field entropic effects*: Model calculations [F. Solal, R. Caudron, F. Ducastelle, A. Finel, and A. Loiseau, Phys. Rev. Lett. **58**, 2245 (1987); C. Wolverton, A. Zunger, and Z.-W. Lu, Phys. Rev. B **49**, 16 058 (1994)] and those for the fcc Madelung lattice [C. Wolverton and A. Zunger, Phys. Rev. B **51**, 6876 (1995)] have shown that in some cases one can have $k_{LRO} = \langle 1\frac{1}{2}0 \rangle$ and $k_{SRO} = \langle 100 \rangle$ due to non-mean-field entropic effects. A mean-field theory would (in principle) be capable of describing the first two types of distinctions, but not the third.

[5] W. Schweika, in *Statics and Dynamics of Alloy Phase Transformations*, Vol. 319 of *NATO Advanced Study Institute, Series B: Physics*, edited by P. E. A. Turchi and A. Gonis (Plenum, New York, 1994), p. 103.

[6] L. Reinhard and S. C. Moss, Ultramicroscopy **52**, 223 (1993).

[7] S. C. Moss, in *Applications of Neutron Scattering to Materials Science*, MRS Symposia Proceedings (Materials Research Society, Pittsburgh, in press).

[8] D. de Fontaine, Acta. Metall. **23**, 553 (1975).

[9] F. J. Pinski, B. Ginatempo, D. D. Johnson, J. B. Staunton, G. M. Stocks, and B. L. Gyorffy, Phys. Rev. Lett. **66**, 766 (1991).

[10] Z.-W. Lu, S.-H. Wei, and A. Zunger, Phys. Rev. Lett. **68**, 1961 (1992), demonstrate that although *relativistic* calculations of Ni-Pt alloys place this system in case (iii) of Table I, *nonrelativistic* Ni-Pt is a case (ii)$_a$ alloy.

[11] Z. W. Lu, S.-H. Wei, and A. Zunger, Phys. Rev. Lett. **68**, 1961 (1992).

[12] P. P. Singh, A. Gonis, and P. E. A. Turchi, Phys. Rev. Lett. **71**, 1605 (1993).

[13] T. B. Wu and J. B. Cohen, Acta Metall. **31**, 1929 (1983).

[14] Z.-W. Lu and A. Zunger, Phys. Rev. B **50**, 6626 (1994).

[15] K. Ohshima, D. Watanabe, and J. Harada, Acta Crystallogr. Sec. A **32**, 883 (1976).

[16] B. L. Gyorffy and G. M. Stocks, Phys. Rev. Lett. **50**, 374 (1983); B. L. Gyorffy, D. D. Johnson, F. J. Pinski, D. M. Nicholson, and G. M. Stocks, in *Alloy Phase Stability*, Vol. E163 of *NATO Advanced Study Institute, Series B: Physics*, edited by G. M. Stocks and A. Gonis (Kluwer, Dordrecht, 1989), p. 421; G. M. Stocks, D. M. C. Nicholson, W. A. Shelton, B. L. Gyorffy, F. J. Pinski, D. D. Johnson, J. B. Staunton, B. Ginatempo, P. E. A. Turchi, and M. Sluiter, in *Statics and Dynamics of Alloy Phase Transformations*, Vol. 319 of *NATO Advanced Study Institute, Series B: Physics*, edited by P. E. A. Turchi and A. Gonis (Plenum, New York, 1994), p. 305.

[17] Z.-W. Lu, D. B. Laks, S.-H. Wei, and A. Zunger, Phys. Rev. B **50**, 6642 (1994).

[18] T. B. Massalski, *Binary Alloy Phase Diagrams* (ASM International, Metals Park, OH, 1986).

[19] A recent review is given by A. Zunger, in *Statics and Dynamics of Alloy Phase Transformations*, Vol. 319 of *NATO Advanced Study Institute, Series B: Physics*, edited by P. E. A. Turchi and A. Gonis (Plenum, New York, 1994), p. 361.

[20] R. Caudron, M. Sarfati, M. Barrachin, A. Finel, F. Ducastelle, and F. Solal, J. Phys. (France) I **2**, 1145 (1992); A. Finel (private communication).

[21] W. Schweika, in *Alloy Phase Stability*, Vol. E163 of *NATO Advanced Study Institute, Series B: Physics*, edited by G. M. Stocks and A. Gonis (Kluwer Academic, Dordrecht, 1989), p. 137.

[22] M. Barrachin, A. Finel, R. Caudron, A. Pasturel, and A. Francois, Phys. Rev. B **50**, 12 980 (1994).

[23] W. Schweika and H. G. Haubold, Phys. Rev. B **37**, 9240 (1988).

[24] V. Gerold and J. Kern, Acta Metall. **35**, 393 (1987).

[25] R. Caudron, M. Sarfati, M. Barrachin, A. Finel, F. Ducastelle, and F. Solal, Physica B **180**, 822 (1992).

[26] F. Solal and A. Finel, in *Alloy Phase Stability and Design*, edited by G. M. Stocks, D. P. Pope, and A. F. Giamei, MRS Symposia Proceedings No. 186 (Materials Research Society, Pittsburgh, 1991), p. 123.

[27] F. Solal, R. Caudron, and A. Finel, Physica B **156**, 75 (1989).

[28] C. Wolverton, A. Zunger, and Z.-W. Lu, Phys. Rev. B **49**, 16 058 (1994).

[29] C. Wolverton and A. Zunger, Phys Rev. B **50**, 10 548 (1994).

[30] D. D. Johnson, J. B. Staunton, and F. J. Pinski, Phys. Rev. B **50**, 1473 (1994).

[31] It should be noted that the fcc alloy $Ni_{0.5}V_{0.5}$ is "fictitious" in the sense that the experimentally assessed Ni-V phase diagram shows fcc solid solution, which extends only from pure Ni to $Ni_{0.57}V_{0.43}$. The assessed Pd-V phase diagram shows stable fcc solid solutions, which extend from pure-Pd to $Pd_{0.42}V_{0.58}$, thus, none of the Pd-V alloys considered here are fictitious.

[32] J. F. Smith, in *Phase Diagrams of Binary Vanadium Alloys* (ASM International, Metals Park, OH, 1987).

[33] F. Solal, R. Caudron, F. Ducastelle, A. Finel, and A. Loiseau, Phys. Rev. Lett. **58**, 2245 (1987).

[34] Several authors have evaluated $\Delta E(T = 0)$ between $L1_2$ and DO_{22} for Ni_3V from first-principles electronic structure calculations [see, e.g., J. H. Xu, T. Oguchi, and A. J. Freeman, Phys. Rev. B **35**, 6940 (1987); S. Pei *et al.*, *ibid.* **39**, 5767 (1989); W. Lin, J. H. Xu, and A. J. Freeman, *ibid.* **45**, 10 863 (1992); Ref. 22]. All these previous studies employed the atomic sphere approximation, gave results which are within a few meV/atom of one another, and agree well with our full-potential results.

[35] In the LAPW calculations presented here for Ni_3V (Pd_3V), we used a cutoff kinetic energy for the LAPW basis functions of 16.7 Ry (14.1 Ry).

[36] (a) O. Eriksson, J. M. Wills, and D. Wallace, Phys. Rev. B **46**, 5221 (1992), showed how S_{el} may be approximately deduced (for several transition metals) from thermophysical measurements by subtracting a quasiharmonic term from the total measured entropy. The residual entropy (for a pure metal, *not* an alloy) is then given by S_{el} plus an anharmonic contribution. This residual entropy may then be compared with calculations of S_{el}. (b) G. Grimvall, J. Häglund, and A. Fernández Guillermet, Phys. Rev. B **47**, 15 338 (1993). (c) P. Turek, R. Kuentzler, A. Bieger, and R. Jesser, Solid State Commun. **53**, 979 (1985).

[37] D. M. C. Nicholson, G. M. Stocks, Y. Wang, W. A. Shelton, Z. Szotek, and W. M. Temmerman, Phys. Rev. B **50**, 14 686 (1994).

[38] G. Grimvall [*Thermophysical Properties of Materials* (Elsevier, New York, 1986), pp. 157–172] has shown that at low temperatures, Eqs. (13) and (14) neglect an electron-phonon many-body enhancement factor, $(1 + \lambda)$, where λ has a typical value of 0.4.

[39] In units of the lattice constant $a = 2$, J_3 has coordinates (000), (110), and (101), while K_4 has coordinates (000), (110), (101), and (200).

[40] D. J. Singh, *Planewaves, Pseudopotentials, and the LAPW Method* (Kluwer, Boston, 1994).

[41] D. M. Ceperley and B. J. Alder, Phys. Rev. Lett. **45**, 566 (1980).

[42] J. P. Perdew and A. Zunger, Phys. Rev. B **23**, 5048 (1981).

[43] S. Froyen, Phys. Rev. B **39**, 3168 (1989).

[44] H. J. Monkhorst and J. D. Pack, Phys. Rev. B **13**, 5188 (1976).

[45] P. Villars and L. D. Calvert, *Pearson's Handbook of Crystallographic Data for Intermetallic Phases* (American Society for Metals, Metal Park, OH 1991).

[46] (a) Z.-W. Lu, B. Klein, and A. Zunger, Phys. Rev. Lett. **75**, 1320 (1995); (b) J. Kudrnovský, I. Turek, A. Pasturel, R. Tetot, V. Drchal, and P. Weinberger, Phys. Rev. B **50**, 9603 (1994).

[47] One form of the energy and entropy associated with electronic excitations used for the one-electron terms in finite-T density-functional theory is

$$\int_{-\infty}^{+\infty} \epsilon\, n(\epsilon)\, f(\epsilon - \mu)\, d\epsilon$$

$$+ kT \int_{-\infty}^{+\infty} n(\epsilon)\, [f \ln f + (1 - f)\ln(1 - f)]\, d\epsilon,$$

while another is

$$-\int_{-\infty}^{+\infty} \int_{-\infty}^{\epsilon} n(\epsilon')\, f(\epsilon - \mu)\, d\epsilon'\, d\epsilon$$

$$+ \mu \int_{-\infty}^{+\infty} \epsilon\, n(\epsilon)\, f(\epsilon - \mu)\, d\epsilon.$$

While the latter form does not immediately appear to contain the *entropy* associated with electronic excitations (due to the absence of explicit "$f \ln f$"-type terms), it can be demonstrated that the two forms are equivalent by integrating by parts twice. [D. D. Johnson (private communication)].